World Journal of Advanced Research and Reviews
eISSN: 2581-9615 CODEN (USA): WJARAI
Cross Ref DOI: 10.30574/wjarr
Journal homepage: https://wjarr.com/

(RESEARCH ARTICLE)

Check for updates

Catalytic Enhancement of LSTN/SDC Anodes for Direct Hydrocarbon Energy Conversion

Mohammad Yousefpour [1,*] and Mahnaz Zameni [2]

[1] *Department of Science, Azad University of Amol, Amol, Iran.*
[2] *Department of Computer Science, Azad University of Sari, Sari, Iran.*

World Journal of Advanced Research and Reviews, 2025, 28(02), 420-428

Publication history: Received on 26 September 2025; revised on 01 November 2025; accepted on 04 November 2025

Article DOI: https://doi.org/10.30574/wjarr.2025.28.2.3735

Abstract

The escalating global demand for energy, coupled with growing environmental concerns, has intensified efforts to develop sustainable and diversified energy solutions. Among various energy conversion devices, solid oxide fuel cells (SOFCs) have garnered significant attention due to their exceptional energy conversion efficiency and ability to utilize hydrocarbon fuels directly. However, conventional SOFC anodes based on Ni/YSZ cermets suffer from critical drawbacks such as carbon deposition and sulfur poisoning when operated with hydrocarbon fuels. To address these limitations, mixed ionic and electronic conducting (MIEC) materials, notably $La_{0.2}Sr_{0.8}Ti_{0.9}Ni_{0.1}O_3$ (LSTN), have emerged as promising alternatives due to their superior carbon and sulfur tolerance, alongside robust thermal and redox stability. This study investigates the electro-oxidation of methanol over a composite anode consisting of LSTN integrated with samarium-doped ceria (SDC). To enhance the electrochemical performance, $LaFe_{0.6}Co_{0.4}O_3$ (LFC) precursor solutions of varying concentrations were impregnated into the composite structure. Impedance spectroscopy results demonstrated that LFC incorporation, particularly when synthesized with ethylene glycol (EG), markedly reduced electrode polarization resistance and improved catalytic activity. X-ray diffraction analysis further confirmed the successful formation of the LFC perovskite phase within the porous anode framework. These findings underscore that LFC-impregnated LSTN/SDC composite anodes, especially those synthesized with EG, significantly enhance the methanol electro-oxidation process, establishing them as strong candidates for high-performance SOFC applications. Overall, this research contributes to advancing the efficiency and durability of solid oxide fuel cells, thereby supporting the transition toward sustainable energy technologies.

Keywords: Solid oxide fuel cell; Anode electrode; LSTN/SDC; Electrochemical impedance spectroscopy; Methanol oxidation; LFC

1. Introduction

The escalating global demand for energy, combined with the substantial environmental repercussions of conventional energy sources, has intensified efforts toward the adoption of sustainable and diversified energy solutions [1-6]. A central objective within this pursuit is the enhancement of energy conversion technologies, particularly solid oxide fuel cells (SOFCs) [7] and advanced batteries [8, 9]. SOFCs, recognized for their outstanding electrochemical conversion efficiency, generate electrical power through redox reactions involving gaseous fuels [10, 11]. Hydrogen serves as the principal fuel for SOFCs, typically obtained via hydrocarbon reforming. Unlike other fuel cell systems, SOFCs possess the unique ability to utilize hydrocarbon fuels directly through internal reforming processes [12, 13]. Liquid hydrocarbon derivatives such as alcohols can be produced sustainably via industrial synthesis routes and biomass conversion methods [14, 15]. Among these, methanol stands out as the simplest alcohol due to its single-carbon structure [16, 17]. The absence of a strong C–C bond in methanol's molecular composition greatly facilitates its

* Corresponding author: Mohammad Yousefpour

reforming process and enables direct use within SOFCs [18, 19]. Moreover, methanol's high hydrogen-to-carbon ratio ensures the generation of a significant hydrogen yield for the anode reaction in SOFCs.

In conventional SOFC configurations, the utilization of Ni/YSZ ($Zr_xY_{1-x}O_2$) cermets have been widely investigated as prospective anode materials owing to their favorable attributes, such as low polarization resistance in hydrogen atmospheres and excellent catalytic performance toward methane steam reforming [20-23]. Nonetheless, several limitations hinder their performance, including poor redox resilience and proneness to coking and sulfur poisoning under hydrocarbon-based operations [24, 25]. Considering the ongoing high cost associated with hydrogen production, substantial research efforts have focused on the design and synthesis of alternative anode compositions to improve fuel compatibility and durability in SOFCs.

Materials exhibiting mixed ionic and electronic conductivity (MIEC) have emerged as strong candidates for next-generation SOFC anodes [26-30]. Notably, ceramic anodes such as double perovskites $Sr_2Mg_{1-x}Mn_xMoO_{6-\delta}$ [31-33], strontium titanate based perovskites such as $(La,Sr)(Ti)O_{3-\delta}$) [34, 35], and lanthanum chromate based perovskites like $(La,Sr)(Cr,Mn)O_{3-\delta}$ [27, 36, 37] have demonstrated encouraging electrochemical and structural characteristics. Among these, $La_{0.2}Sr_{0.8}Ti_{0.9}Ni_{0.1}O_3$ (LSTN) has drawn significant attention as a promising anode material due to its remarkable resistance to carbon deposition, sulfur contamination, and degradation under redox and thermal cycling conditions. LSTN perovskite-based anodes exhibit superior structural stability and electrochemical performance under both hydrogen and methane environments, attributed to optimized Ni ex-solution behavior and tailored microstructural features achieved through precise control of firing temperature and atmospheric conditions [38]. Park and Choi [38] demonstrated that LSTN sintered at 1250 °C under a hydrogen atmosphere delivered optimal performance in ScSZ electrolyte-supported SOFCs, where the synergistic effects of favorable microstructure and active Ni ex-solution enabled a peak power density of approximately 130 mW cm^{-2} at 800 °C in wet H_2. Similarly, Lee et al. [39] explored LST infiltration into porous YSZ frameworks for SOFC anodes, revealing that calcination temperature plays a pivotal role in determining the resulting microstructure and electrical conductivity of the LST–YSZ composite. Cells incorporating anodes calcined at 1373 K achieved the highest electrical conductivity (>0.4 S cm^{-1}) and enhanced electrochemical output relative to those treated at higher temperatures, primarily due to reduced particle coarsening and improved pore interconnectivity [39].

In parallel with advancements in thin-film fabrication aimed at tuning electrode material properties [26, 40, 41], a highly effective approach to improving SOFC electrode performance involves the impregnation of oxide or noble metal nanoparticles into the electrode matrix [42, 43]. For instance, Kim et al. [44] evaluated the operational stability of composite LSCM/YSZ anodes incorporating Pt, Pd, and Ni nanoparticles under dry methane conditions. Their results indicated that anodes containing Ni and Pt underwent severe carbon deposition, resulting in performance degradation due to coking effects. More recently, $LaFe_{0.7}Co_{0.3}O_{3-\delta}$ perovskite has gained attention as a promising candidate for symmetric SOFC electrodes [45]. This material exhibits high electrocatalytic activity for both hydrogen oxidation and oxygen reduction reactions. At 750 °C, a symmetric LFC/$Sm_{0.2}Ce_{0.8}O_{1.9}$ (SDC) electrode demonstrated a peak power density of 0.291 W cm^{-2}. Additionally, Rostaghi Chalaki et. al. [27] reported that impregnation of LFC nanoparticles into LSCM/YSZ composite anodes significantly lowered electrode polarization losses.

The present study focuses on the electro-oxidation of methanol on a composite anode composed of LSTN and SDC. To enhance electrode performance, $LaFe_{0.6}Co_{0.4}O_3$ (LFC) precursor solutions of varying concentrations were infiltrated into the LSTN/SDC composite, followed by testing under a humidified CH_3OH environment. Electrochemical analyses were conducted to elucidate the methanol oxidation mechanism on the modified anode surface. Furthermore, detailed microstructural characterization was performed on both pristine and LFC-impregnated samples to assess morphological and structural changes induced by the impregnation process.

2. Experimental

Electrolyte pellets were fabricated by cold pressing a mixture comprising 1 g of SDC powder and PVB binder, followed by sintering at 1250 °C for 5 hours. The sintered SDC pellets exhibited a final diameter of approximately 14 mm and a thickness of about 0.9 mm. To remove surface impurities and achieve uniform surface roughness, the pellets were gently ground prior to electrode application. A Pt paste was applied at the center of each SDC pellet to serve as the counter electrode with an active area of 0.5 cm^2, while the reference electrode was patterned as a concentric ring. Both electrodes were subsequently heat-treated in air at 900 °C for 1 hour to ensure adequate adhesion and conductivity.

For the anode electrode preparation, a composite powder consisting of LSTN and SDC was synthesized by roll-milling in ethanol for 10 hours at a 1:1 weight ratio to ensure compositional homogeneity. The resulting mixture was dried and combined with an ink vehicle to produce a printable LSTN/SDC slurry. This slurry was uniformly coated on the opposite

side of the counter electrode and sintered in air at 1200 °C for 4 hours. The resulting anode layer exhibited a surface area of 0.5 cm^2 and a final thickness of approximately 30 μm after sintering.

For nanoparticle impregnation, LFC precursor solutions were synthesized by dissolving stoichiometric quantities of $La(NO_3)_3 \cdot 6H_2O$, $Fe(NO_3)_3 \cdot 9H_2O$, and $Co(NO_3)_2 \cdot 6H_2O$ (Merck, Germany) in distilled water, maintaining a molar ratio of 1:0.6:0.4. Solutions of varying LFC concentrations, 0.2 M, 0.3 M, and 0.4 M, were prepared. Ethylene glycol (EG) was introduced as a complexing agent in a 2.5:1 molar ratio relative to total metal ions. Two solution variants were prepared: P-LFC (with EG) and S-LFC (without EG). Controlled droplets of each solution were carefully deposited onto the surface of the LSTN/SDC composite anode. Following impregnation, the electrode surfaces were gently wiped and air-dried before undergoing thermal treatment at 900 °C for 2 hours in air.

Both 0.3 M S-LFC and P-LFC samples were also dried and calcined independently at 900 °C for 2 hours under air, following the procedure outlined by Rostaghi Chalaki et al. [27], to obtain reference LFC nanoparticles. The structural features of the calcined powders were analyzed by X-ray diffraction (XRD) using a Philips PW 1730 diffractometer operated at room temperature with Cu-Kα radiation (λ = 1.5406 Å). Scans were conducted over a 2θ range of 20°–80° with 0.02° step increments. The surface morphology and particle dispersion of the impregnated LSTN/SDC composites were examined using field-emission scanning electron microscopy (FESEM, TESCAN MIRA3).

Electrochemical characterization was performed using a three-electrode configuration. Platinum paste served as the current collector on the anode surface, and Pt wires were used as current leads. Methanol vapor was employed as the fuel, while the counter and reference electrodes were exposed to ambient air. Prior to measurements, all anodes were activated at 800 °C in methanol for 1 hour to stabilize their electrocatalytic behavior. Electrochemical impedance spectroscopy (EIS) analyses were carried out with an Autolab PGSTAT302 system at open circuit potential (OCP) over a frequency range of 0.01 Hz to 100 kHz. The electrode polarization resistance (R_E) and ohmic resistance (R_Ω) were extracted and analyzed using ZView software

3. Results and discussion

3.1. Phase Characterization

Figure 1 presents the XRD results for the S-LFC and P-LFC powders following calcination in air at 900 °C. The XRD spectrum of the S-LFC sample revealed diffraction peaks corresponding to $LaFeO_3$, $LaCoO_3$, La_2O_3, and Fe_2O_3 phases, indicating that the desired LFC perovskite phase did not form under these conditions. In contrast, the P-LFC powder exhibited diffraction features characteristic of the orthorhombic $LaFe_{0.6}Co_{0.4}O_3$ structure (JCPDS card no. 00-044-0361), with no extraneous Bragg reflections beyond those associated with the target perovskite phase. This observation suggests that the LFC perovskite phase successfully formed when EG was used during synthesis and is also likely generated within the porous framework of the LSTN/SDC composite anode following impregnation with the P-LFC solution.

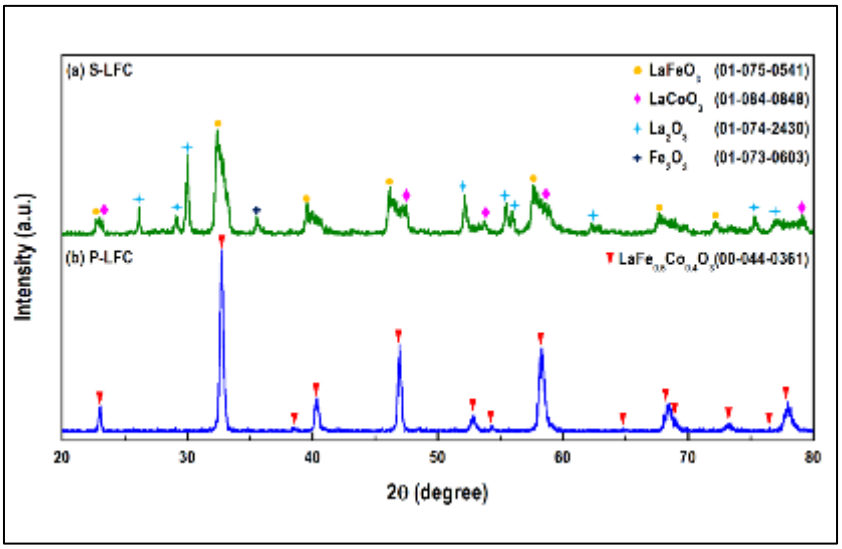

Figure 1 XRD patterns of S-LFC and P-LFC solutions calcined at 900 °C for 2 h in air

3.2. Electrochemical Measurements

Figure 2a displays the impedance spectrum of the LSTN/SDC composite anode recorded at OCP and 800 °C under a methanol atmosphere. To elucidate the impedance behavior associated with methanol electro-oxidation on the LSTN/SDC composite anode, equivalent circuit modeling was applied. The impedance spectra were fitted using the $R_\Omega(RQ)_h(RQ)_m(RQ)_l$ circuit model, where R_Ω represents the total ohmic resistance of the cell. The parameters R_h, R_m, and R_l correspond to the electrode polarization resistances at high, intermediate, and low frequencies, respectively, and their sum yields the overall electrode polarization resistance ($R_E = R_h + R_m + R_l$). The associated constant phase elements Q_h, Q_m, and Q_l were included to account for the non-ideal capacitive behavior in each frequency regime, as illustrated in Figure 2b.

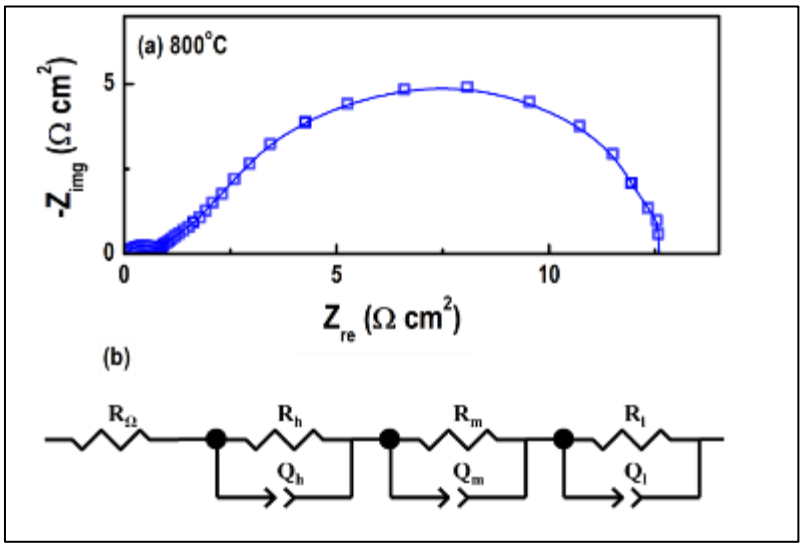

Figure 2 (a) LSTN/SDC composite anode electrode polarization resistance at 800 °C in methanol. Points are experimental data, and the solid line is fitted data with the equivalent circuit $R_\Omega(RQ)_h(RQ)_m(RQ)_l$. (b) Equivalent circuit model for fitting the impedance spectra of the LSTN/SDC composite anodes

At 750 °C, the electrode polarization resistance associated with methanol oxidation was measured as 17.81 Ω·cm^2. With increasing temperature to 800 and 850 °C, the R_E values decreased to 12.62 and 8.30 Ω·cm^2, respectively, indicating enhanced electrochemical activity at elevated temperatures. The fitted results derived from the impedance spectra are summarized in Table 1. The 'n' parameter corresponding to each frequency arc was first determined from the impedance fitting of the LSTN/SDC composite anode at 750 °C and subsequently held constant for fittings conducted at 800 and 850 °C. To further elucidate the methanol oxidation mechanism, the activation energy associated with each semicircular arc was evaluated. The activation energies for the high-, medium-, and low-frequency processes were calculated as 1.16, -0.095, and 0.92 eV, respectively. These findings suggest that both the high- and low-frequency processes are thermally activated, whereas the medium-frequency response exhibits slight thermal deactivation.

Table 1 Fitted impedance results for the methanol oxidation reaction on the LSTN/SDC composite anode at different temperatur**es**

Temp. (°C)	Ohmic resistance (Ω cm²)	High frequency			Medium frequency			Low frequency		
		R_h (Ω cm²)	Q_h (Ω cm² s^n)	n_h	R_m (Ω cm²)	Q_m (Ω cm² s^n)	n_m	R_l (Ω cm²)	Q_l (Ω cm² s^n)	n_l
750	5.65	1.97	8.5×10^{-4}	0.98	1.89	0.22	0.67	14.03	0.16	1
800	4.92	1.28	6.5×10^{-4}	0.98	2.09	0.24	0.67	9.25	0.14	1
850	3.81	0.77	4.8×10^{-4}	0.98	2.35	0.28	0.67	5.20	0.18	1

Jiang et al. [46] investigated the methane oxidation reaction on an LSCM/YSZ composite anode under wet methane conditions and identified three distinct impedance arcs in their spectra. They attributed the high-frequency arc to the transfer of charged species across the LSCM/YSZ interfacial region. In a separate study, a comparative analysis between

the $La_{0.4}Sr_{0.6}Ti_{1-x}Mn_xO_{3-\delta}$ anode and its composite counterpart, $La_{0.4}Sr_{0.6}Ti_{1-x}Mn_xO_{3-\delta}$/YSZ, revealed that the composite configuration exhibited a markedly smaller high-frequency arc relative to the single-phase anode. This observation was ascribed to the enlarged interfacial area between $La_{0.4}Sr_{0.6}Ti_{1-x}Mn_xO_{3-\delta}$ and YSZ, interface area, which facilitated more efficient charge transfer processes [47]. Given the correspondence of high-frequency arc behavior with those findings [46, 47], it can be inferred that the high-frequency response observed in this study similarly arises from charge transfer phenomena at the LSTN/SDC interface.

Primdahl and Mogensen [48] examined the electrochemical oxidation of humidified hydrogen on a Ni/YSZ electrode using a three-electrode setup at 1000 °C. Their impedance spectra featured a distinct arc centered around 1 Hz, characterized by a small negative activation energy (-0.09 eV), which they attributed to gas conversion reactions occurring on the Ni/YSZ electrode surface. It is noteworthy that the gas composition at the anode electrode differs fundamentally from that at the counter and reference electrodes. In the present study, the medium-frequency arc observed at 800 °C exhibited a peak frequency of 0.55 Hz and an activation energy of -0.095 eV. Comparison with previous reports suggests that this medium-frequency response is associated with surface gas conversion reactions occurring on the LSTN/SDC composite anode.

Jiang et al. [49] further analyzed the impedance spectra of a Ni/YSZ anode operating in wet hydrogen at 850 °C. Their results revealed a low-frequency arc with a peak near 0.02 Hz and an activation energy of 0.42 eV, attributed to the dissociative adsorption of hydrogen on Ni particles. The observed thermal activation of this process aligns with the characteristics of the low-frequency arc in the present investigation, indicating that this feature corresponds to hydrogen dissociative adsorption occurring on the surface of the LSTN/SDC composite anode [49].

3.3. LFC solutions impregnation

Figure 3 illustrates the effect of varying S-LFC and P-LFC solution concentrations on the electrochemical performance of the LSTN/SDC composite electrode at 800 °C in a methanol atmosphere. When impregnated with a 0.2 M P-LFC solution, the LSTN/SDC electrode exhibited a high-frequency arc with a peak frequency exceeding 10 kHz, which was entirely displaced below the real axis on the Nyquist plot. In contrast, impregnation with a 0.1 M S-LFC solution significantly reduced the electrode polarization resistance from 12.62 to 6.97 $\Omega \cdot cm^2$. Further increases in the S-LFC concentration to 0.2 M and 0.3 M led to additional reductions in R_E, reaching 5.08 and 6.31 $\Omega \cdot cm^2$, respectively. This decline in polarization resistance can be ascribed to enhanced catalytic behavior and improved ionic–electronic transport within the LSTN/SDC composite anode, facilitated by LFC incorporation.

Similarly, when P-LFC solutions with concentrations of 0.1 M, 0.2 M, and 0.3 M were used, the polarization resistance further decreased to 4.45, 2.53, and 3.11 $\Omega \cdot cm^2$, respectively. The superior performance observed for P-LFC–impregnated electrodes is attributed to the presence of EG as a complexing agent during synthesis, which promotes the formation of the LFC perovskite phase. Given that LFC exhibits higher intrinsic catalytic activity than $LaFeO_3$ and $LaCoO_3$, the pronounced reduction in polarization resistance reflects the improved electrochemical kinetics induced by the P-LFC impregnation process.

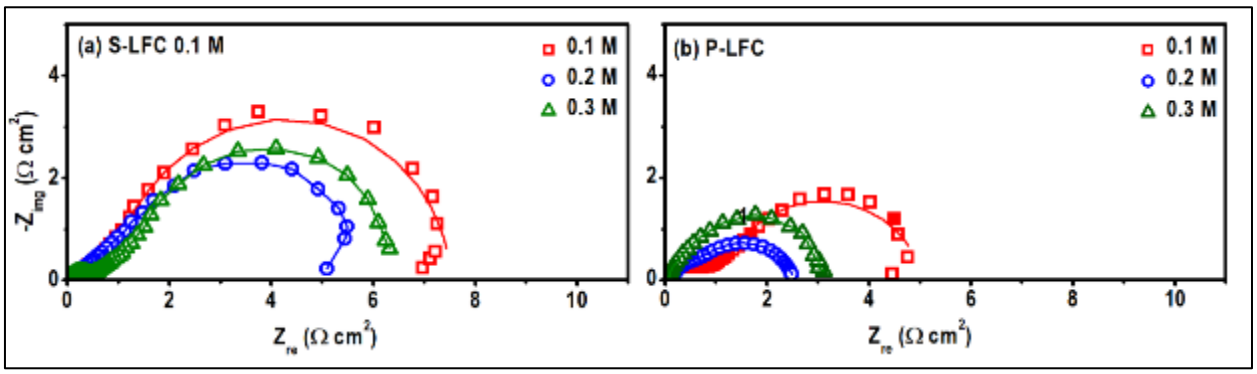

Figure 3 Impedance spectra of LSTN/SDC composite anodes at different S-LFC and P-LFC solutions concentrations in methanol at 800 °C. Points are experimental data and solid lines are fitted data with the equivalent circuit. Closed symbols mark the frequency points from 0.01 Hz to 100 kHz at each frequency decade

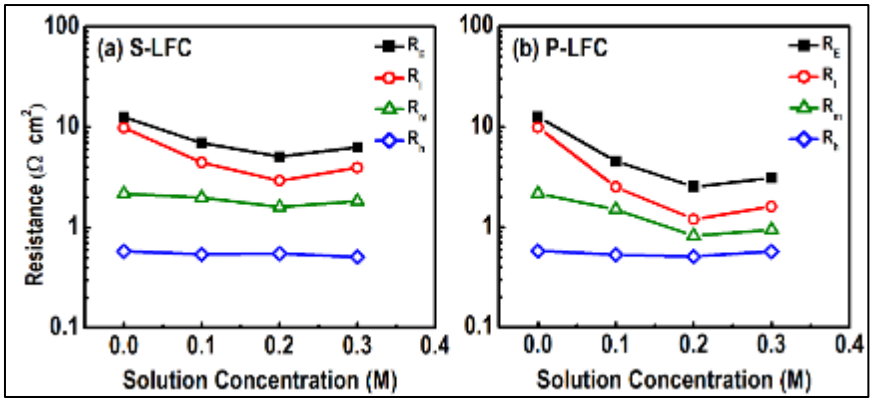

Figure 4 The effect of S-LFC and P-LFC solutions concentration on R_h, R_m, R_l and R_E of LSTN/SDC composite anode in methanol. Closed points are experimental data and open points are fitting results

Figure 4 depicts the influence of S-LFC and P-LFC solution concentrations on the electrode polarization resistance and the corresponding high-, medium-, and low-frequency arcs. A significant reduction in polarization resistance was observed for the LSTN/SDC composite anode during methanol electro-oxidation following impregnation with both LFC solutions. This improvement primarily originates from decreases in the medium- and low-frequency resistive components. For the pristine LSTN/SDC composite anode at 800 °C, the low-frequency resistance (R_3) was measured at 9.25 Ω·cm², which decreased to 2.93 and 1.20 Ω·cm² upon impregnation with 0.2 M S-LFC and P-LFC solutions, respectively. The decline in low-frequency resistance is ascribed to enhanced catalytic activity toward hydrogen adsorption induced by LFC incorporation. Notably, the P-LFC-impregnated sample exhibited a more substantial reduction in R3 than the S-LFC-impregnated one, exceeding a two-fold improvement.

At medium frequencies, the electrode polarization resistance decreased from 2.09 Ω·cm² to 1.60 Ω·cm² and 0.82 Ω·cm² following impregnation with 0.2 M S-LFC and P-LFC solutions, respectively. Similar to the behavior observed at low frequencies, P-LFC treatment yielded a more pronounced improvement, likely due to the superior catalytic activity of the LFC perovskite in facilitating methanol decomposition. In contrast, the high-frequency resistance exhibited only minor variations upon impregnation with either solution, suggesting that ionic conductivity within the anode matrix remained relatively unaffected. However, at higher impregnation concentrations (0.3 M), a notable increase in polarization resistance was detected, presumably resulting from non-uniform nanoparticle distribution within the porous LSTN/SDC framework.

The corresponding SEM micrographs in Figure 5 display the morphology of the LSTN/SDC composite anode before and after impregnation with 0.2 M S-LFC and P-LFC solutions. The microstructural analysis revealed the formation of finely dispersed nanoparticles on the anode surface following impregnation. Particle size evaluation using Digimizer software determined an average LFC nanoparticle diameter of approximately 86 nm for the 0.2 M P-LFC sample. The P-LFC-impregnated anode exhibited more homogeneous nanoparticle formation compared to that treated with the S-LFC solution. As previously discussed, the lowest overall polarization resistance (R_E) was observed for the 0.2 M P-LFC–impregnated anode. This enhanced performance can be attributed to the uniform dispersion and optimized integration of catalytically active LFC nanoparticles within the porous LSTN/SDC network.

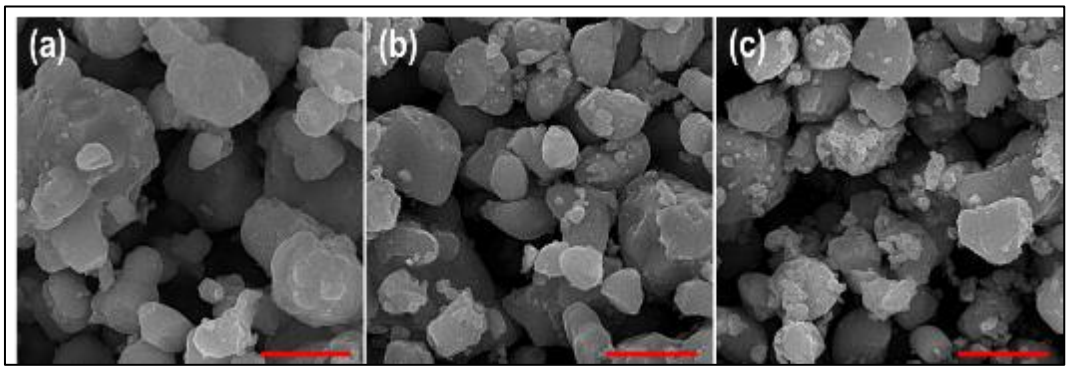

Figure 5 SEM images of LSTN/SDC composite anode electrode, (a) before, and after impregnation with 0.2 M of (b) S-LFC and (c) P-LFC solutions. The red line is scale bar and equals 1 micron

4. Conclusion

In conclusion, the LSTN/SDC composite anode exhibited notable electrode polarization resistance during methanol electro-oxidation at 800 °C. Impedance spectral analysis using an equivalent circuit model indicated that the reaction mechanism involves at least three distinct electrode processes: charge transfer at high frequencies, gas conversion at intermediate frequencies, and hydrogen dissociative adsorption at low frequencies on the LSTN/SDC surface. The impregnation of LFC solutions markedly reduced the overall polarization resistance of the composite anode. This enhancement is attributed to the formation of catalytically active LFC nanoparticles, which improve electrochemical activity by promoting methanol decomposition and facilitating hydrogen adsorption. The optimal reduction in polarization resistance was achieved with 0.2 M LFC impregnation, while higher concentrations (0.3 M) resulted in increased resistance, likely due to non-uniform nanoparticle dispersion within the porous LSTN/SDC network.

Compliance with ethical standards

Acknowledgments

The author would like to thank the Azad University of Amol. This study did not receive funding from any government or private agency.

Disclosure of conflict of interest

The author has no conflict of interest in this study.

References

[1] Taghavi, H., Liquid Cooling System for a High Power, Medium Frequency, and Medium Voltage Isolated Power Converter. 2023, University of South Carolina: United States -- South Carolina. p. 74.

[2] Taghavi, H., A. El Shafei, and A. Nasiri. Liquid Cooling System for a High Power, Medium Frequency, and Medium Voltage Isolated Power Converter. in 2023 12th International Conference on Renewable Energy Research and Applications (ICRERA). 2023. IEEE.

[3] Bhuvela, P., H. Taghavi, and A. Nasiri. Design Methodology for a Medium Voltage Single Stage LLC Resonant Solar PV Inverter. in 2023 12th International Conference on Renewable Energy Research and Applications (ICRERA). 2023. IEEE.

[4] Shirvani, S.M.N., et al., Optimal design of a composite sandwich panel with a hexagonal honeycomb core for aerospace applications. Iranian Journal of Science and Technology, Transactions of Mechanical Engineering, 2023. **47**(2): p. 557-568.

[5] Yousefpour, K., et al. Control of Grid-Connected Inverters Using PLL for Synchronization and Harmonic Mitigation. in 2025 IEEE Texas Power and Energy Conference (TPEC). 2025. IEEE.

[6] Varnousfaderani, S.A., et al. Real-World Evaluation of Compressed Sensing for Data Compression in Smart Grids. in 2025 IEEE Texas Power and Energy Conference (TPEC). 2025. IEEE.

[7] Fan, L., et al., Nanomaterials and technologies for low temperature solid oxide fuel cells: recent advances, challenges and opportunities. Nano Energy, 2018. **45**: p. 148-176.

[8] Jeena, M., et al., A siloxane-incorporated copolymer as an in situ cross-linkable binder for high performance silicon anodes in Li-ion batteries. Nanoscale, 2016. **8**(17): p. 9245-9253.

[9] Bhuvela, P., H. Taghavi, and A. Nasiri, Loss Analysis of a Resonant Converter Based Medium Voltage Single Stage Solar PV Inverter. IEEE Transactions on Industry Applications, 2025.

[10] Lee, K.T. and E.D. Wachsman, Role of nanostructures on SOFC performance at reduced temperatures. Mrs Bulletin, 2014. **39**(9): p. 783-791.

[11] Taghavi, H., et al. Design and Optimization of a Forced-Air Cooling System for a Compact Medium Voltage Solar Photovoltaic Inverter. in 2024 13th International Conference on Renewable Energy Research and Applications (ICRERA). 2024. IEEE.

[12] Ge, X.M., et al., Solid oxide fuel cell anode materials for direct hydrocarbon utilization. Advanced Energy Materials, 2012. **2**(10): p. 1156-1181.

[13] Taghavi, H., S. Raghu, and J.A. Khan. Optimization of Thermal Management in Power Electronics by the Design of Split Channel Cooling Systems Through Numerical Simulations. in Heat Transfer Summer Conference. 2024. American Society of Mechanical Engineers.

[14] Atkinson, A., et al., Advanced anodes for high-temperature fuel cells. Nature materials, 2004. **3**(1): p. 17-27.

[15] Sun, R., et al., Crystallization Behavior and Luminescence of Inkjet Printing CH3NH3PbBr3. Crystal Research and Technology, 2021. **56**(8): p. 2100004.

[16] Li, H., et al. C2H6 Dehydrogenation and Electrical Power Production in a Protonic Conducting Fuel Cell with in-Situ Exsolved Metal Nanoparticle Catalyst. in Electrochemical Society Meeting Abstracts 239. 2021. The Electrochemical Society, Inc.

[17] Bhuvela, P., H. Taghavi, and A. Nasiri. 13.8 kV, 1MW Resonant Direct AC Medium Voltage Single Stage Solar PV Inverter. in 2024 IEEE Applied Power Electronics Conference and Exposition (APEC). 2024. IEEE.

[18] Sá, S., et al., Catalysts for methanol steam reforming—A review. Applied Catalysis B: Environmental, 2010. **99**(1-2): p. 43-57.

[19] Du, Y., et al., Preparation and thermoelectric properties of graphite/poly (3, 4-ethyenedioxythiophene) nanocomposites. Energies, 2018. **11**(10): p. 2849.

[20] McIntosh, S. and R.J. Gorte, Direct hydrocarbon solid oxide fuel cells. Chemical reviews, 2004. **104**(10): p. 4845-4866.

[21] Jia-Yue, X., et al., Growth and characterization of all-inorganic perovskite CsPbBr3 crystal by a traveling zone melting method. Journal of Inorganic Materials, 2018. **33**(11): p. 1253-1258.

[22] Wang, M., et al., Nanostructured carbon as highly efficient and stable anodes for ethylene production and power generation in protonic ceramic electrochemical cells. Carbon, 2022. **199**: p. 379-386.

[23] Wang, W., et al., Improving the performance for direct electrolysis of CO 2 in solid oxide electrolysis cells with a Sr 1.9 Fe 1.5 Mo 0.5 O 6− δ electrode via infiltration of Pr 6 O 11 nanoparticles. Journal of Materials Chemistry A, 2023. **11**(16): p. 9039-9048.

[24] Su, C., et al., Progress and prospects in symmetrical solid oxide fuel cells with two identical electrodes. Advanced Energy Materials, 2015. **5**(14): p. 1500188.

[25] Wang, M., et al., Improved Solid-State Reaction Method for Scaled-Up Synthesis of Ceramic Proton-Conducting Electrolyte Materials. ACS Applied Energy Materials, 2023. **6**(15): p. 8316-8326.

[26] Yang, G., et al., Tuning Ionic Conductivity in Fluorite Gd-Doped CeO2-Bixbyite RE2O3 (RE= Y and Sm) Multilayer Thin Films by Controlling Interfacial Strain. ACS Applied Electronic Materials, 2023. **5**(8): p. 4556-4563.

[27] Rostaghi Chalaki, H., et al., LaFe 0.6 Co 0.4 O 3 promoted LSCM/YSZ anode for direct utilization of methanol in solid oxide fuel cells. Ionics, 2020. **26**: p. 1011-1018.

[28] Burnwal, S.K., S. Bharadwaj, and P. Kistaiah, Review on MIEC cathode materials for solid oxide fuel cells. Journal of Molecular and Engineering Materials, 2016. **4**(02): p. 1630001.

[29] Park, K.-Y., et al. A Highly Performing Electrode with in-Situ Exsolved Nanoparticles for Direct Electrolysis of CO2. in Electrochemical Society Meeting Abstracts 242. 2022. The Electrochemical Society, Inc.

[30] Wang, W., et al. Rational Identification of Doping Strategy to Achieve a Highly Conductive and Reliable Protonic Electrolyte for Electrochemical Cells. in Electrochemical Society Meeting Abstracts 239. 2021. The Electrochemical Society, Inc.

[31] Huang, Y.-H., et al., Double perovskites as anode materials for solid-oxide fuel cells. Science, 2006. **312**(5771): p. 254-257.

[32] Li, H., et al., Improved cell performance and sulphur tolerance using A-site substituted Sr2Fe1. 4Ni0. 1Mo0. 5O6–δ anodes for solid-oxide fuel cells. Clean Energy, 2023. **7**(1): p. 70-83.

[33] Li, H., et al. A-Site Doping Effect on the Performance of Sr2Fe1. 4 Ni0. 1Mo0. 5O6-Δ Anodes for SOFCs. in Electrochemical Society Meeting Abstracts 242. 2022. The Electrochemical Society, Inc.

[34] Marina, O.A., N.L. Canfield, and J.W. Stevenson, Thermal, electrical, and electrocatalytical properties of lanthanum-doped strontium titanate. Solid State Ionics, 2002. **149**(1-2): p. 21-28.

[35] Lin, J., et al., Atmospheric plasma spraying to fabricate metal-supported solid oxide fuel cells with open-channel porous metal support. Journal of the American Ceramic Society, 2023. **106**(1): p. 68-78.

[36] Li, H., et al., Unlocking the Potential of A-Site Ca-Doped LaCo0. 2Fe0. 8O3− δ: A Redox-Stable Cathode Material Enabling High Current Density in Direct CO2 Electrolysis. ACS Applied Materials & Interfaces, 2023. **15**(37): p. 43732-43744.

[37] Park, K.-Y., et al., High-performance Ruddlesden–Popper perovskite oxide with in situ exsolved nanoparticles for direct CO 2 electrolysis. Journal of Materials Chemistry A, 2023. **11**(39): p. 21354-21364.

[38] Park, B.H. and G.M. Choi, Effect of anode firing on the performance of lanthanum and nickel co-doped SrTiO3 (La0. 2Sr0. 8Ti0. 9Ni0. 1O3− δ) anode of solid oxide fuel cell. Journal of Power Sources, 2015. **293**: p. 684-691.

[39] Lee, S., et al., SOFC anodes based on infiltration of La0. 3Sr0. 7TiO3. Journal of the Electrochemical Society, 2008. **155**(11): p. B1179.

[40] El Loubani, M., et al., Creation of submicron-scale metal oxide speckle patterns on single carbon fibers by a thermodynamically and kinetically controlled nonequilibrium process. Materials & Design, 2025. **250**: p. 113582.

[41] Loubani, M.E., et al., Multifunctional Electrocatalysts for Low-temperature Solid Oxide Fuel Cells. 2024.

[42] Chalaki, H.R., et al. The Effect of Impregnation of Ceramic Nano-particles on the Performance of LSCM/YSZ Anode Electrode of Solid Oxide Fuel Cell. in 5th International Conference on Materials Engineering and Metallurgy. 2016.

[43] Ye, Y., et al., Pd-promoted La0. 75Sr0. 25Cr0. 5Mn0. 5O3/YSZ composite anodes for direct utilization of methane in SOFCs. Journal of the Electrochemical Society, 2008. **155**(8): p. B811.

[44] Kim, J.-S., et al., A study of the methane tolerance of LSCM–YSZ composite anodes with Pt, Ni, Pd and ceria catalysts. Scripta Materialia, 2011. **65**(2): p. 90-95.

[45] Shen, J., et al., Impregnated LaCo0. 3Fe0. 67Pd0. 03O3-δ as a promising electrocatalyst for "symmetrical" intermediate-temperature solid oxide fuel cells. Journal of Power Sources, 2016. **306**: p. 92-99.

[46] Jiang, S.P., et al., (La0. 75Sr0. 25)(Cr0. 5Mn0. 5) O3/YSZ composite anodes for methane oxidation reaction in solid oxide fuel cells. Solid State Ionics, 2006. **177**(1-2): p. 149-157.

[47] Fu, Q., F. Tietz, and D. Stöver, La0. 4Sr0. 6Ti1− x Mn x O3− δ perovskites as anode materials for solid oxide fuel cells. Journal of the Electrochemical Society, 2006. **153**(4): p. D74.

[48] Primdahl, S. and M. Mogensen, Gas conversion impedance: a test geometry effect in characterization of solid oxide fuel cell anodes. Journal of the electrochemical Society, 1998. **145**(7): p. 2431.

[49] Jiang, S., W. Wang, and Y. Zhen, Performance and electrode behaviour of nano-YSZ impregnated nickel anodes used in solid oxide fuel cells. Journal of power sources, 2005.